Mineralogy and Petrology (2024) 118:71–88
https://doi.org/10.1007/s00710-023-00844-z

RESEARCH

Noble and base metal geochemistry of late- to post-orogenic mafic dykes from central Spain

David Orejana[1] · María García-Rodríguez[1] · Cristina de Ignacio[1] · Sergio Ruiz-Molina[1]

Received: 24 February 2023 / Accepted: 13 August 2023 / Published online: 8 September 2023

Abstract

The post-tectonic and post-orogenic mafic rocks from the Spanish Central System (SCS) (Iberian Massif) include dyke swarms of shoshonitic (microgabbros) and alkaline (lamprophyres and diabases) geochemical affinity, which register the nature of the metasomatic lithospheric mantle under central Spain. Such magmas sometimes show a direct (or indirect) relationship with the formation of orogenic and intrusion-related gold deposits, which are relatively abundant in the Iberian Massif. The noble and base metal composition of these intrusions shows Primitive Mantle-normalized patterns characterized by positive Au and Co anomalies and fractionated platinum group elements (PGE): from lower Ir-group PGE (IPGE; Ir–Ru) to higher Pd-group PGE (PPGE; Rh–Pt–Pd). The low contents of PGE, together with the base metal contents of pyrite (which is the dominant sulphide phase in the alkaline dykes), is in accordance with low degrees of mantle partial melting and the early segregation of sulphides during magma differentiation. The scarcity of PGE mineral deposits in the Iberian Massif could be explained in part by the apparent lack of PGE enrichment in the Iberian lithospheric mantle. On the contrary, the positive Au anomaly of the SCS mafic dykes represents relatively high Au contents, similar to (and higher than) those of mafic rocks derived from metasomatized subcontinental lithospheric mantle underlying Au-endowed cratons. Several geochemical features point to subduction-related metasomatism of either oceanic or continental nature as the main source of Au enrichment. The Au re-fertilization of the lithospheric mantle under central Spain makes it a potential source in the formation of gold mineralizations.

Keywords Platinum group elements · Gold endowment · Mantle metasomatism · Central Iberian Zone · Alkaline lamprophyres · Shoshonitic magmas

Introduction

Platinum Group Elements (PGE) mineral deposits have a direct relationship with the generation of mantle-derived mafic magmas (Naldrett 2004; Mungall 2007; Mungall and Naldrett 2008, and references therein), but their formation requires specific favourable conditions during mantle partial melting and subsequent magma evolution, in order to achieve substantial PGE concentrations (e.g., Mungall 2002; Maier et al. 2003; Naldrett 2004; Kinnaird et al. 2005; Sá et al. 2005; Mungall and Brenan 2014). On the other hand, the generation of gold mineral deposits can be associated to fairly different processes (magmatic, hydrothermal and sedimentary) and geological contexts, the most significant of which are the collisional, supra-subduction and Witwatersrand-type settings (e.g., Frimmel 2008). Although Au ores are mainly hosted in the crust and intermediate to felsic magmas frequently play a direct or indirect role in their formation (e.g., Hronsky et al. 2012; Groves et al. 2020), an increasing number of studies have highlighted the apparent connection between these deposits and the presence of an underlying noble metal-enriched subcontinental lithospheric mantle (e.g., Tassara et al. 2017; Holwell et al. 2019; Wang et al. 2020; Schettino et al. 2022). Similar conclusions have been drawn for PGE mineralizations (e.g., Alard et al. 2011; Akizawa et al. 2017).

Post-tectonic and/or post-orogenic mafic melts generated from a metasomatized subcontinental lithospheric mantle may show a spatial, time or genetic relationship with gold mineral deposits

Editorial handling: L. Bindi

✉ David Orejana
dorejana@ucm.es

[1] Departamento de Mineralogía y Petrología, Universidad Complutense de Madrid). C/ José Antonio Novais, Madrid 28040, Spain

(e.g., orogenic and intrusion-related; Müller and Groves 2019). Such magmatic intrusive bodies are often volatile-rich silica undersaturated alkaline rocks of potassic or shoshonitic geochemical affinity (e.g., lamprophyres). When large enough, they may be relevant in ore genesis because they can promote hydrothermal circulation and crustal partial melting (e.g., Heidari et al. 2015). A similar connection between alkaline-shoshonitic mafic magmas and PGE deposits is rare, although a few examples have been documented (Barnes et al. 2008; Graham et al. 2017). In any case, the noble metal abundance in mantle-derived magmas is of key relevance when trying to establish the PGE and gold mineralizing potential of the lithospheric mantle under cratonic areas (e.g., Wang et al. 2020; Choi et al. 2020).

The Iberian Massif, which is part of the collisional European Variscan Belt, is characterized by the presence of abundant late-tectonic intrusion-related and orogenic gold deposits (e.g., Romer and Kroner 2018), and scarce PGE mineralizations (e.g., Piña et al. 2008) (Fig. 1a). Moreover, this terrane was crosscut by post-collisional mantle-derived magmas, which intruded mostly during the subsequent late-tectonic to post-tectonic extensional stages. These features make this terrane a suitable scenario for the study of the relationship between upper mantle geochemistry and noble metals mineral deposit generation in the upper crust.

The Spanish Central System (SCS) mountain range, located in central Iberia, offers one of the best examples of

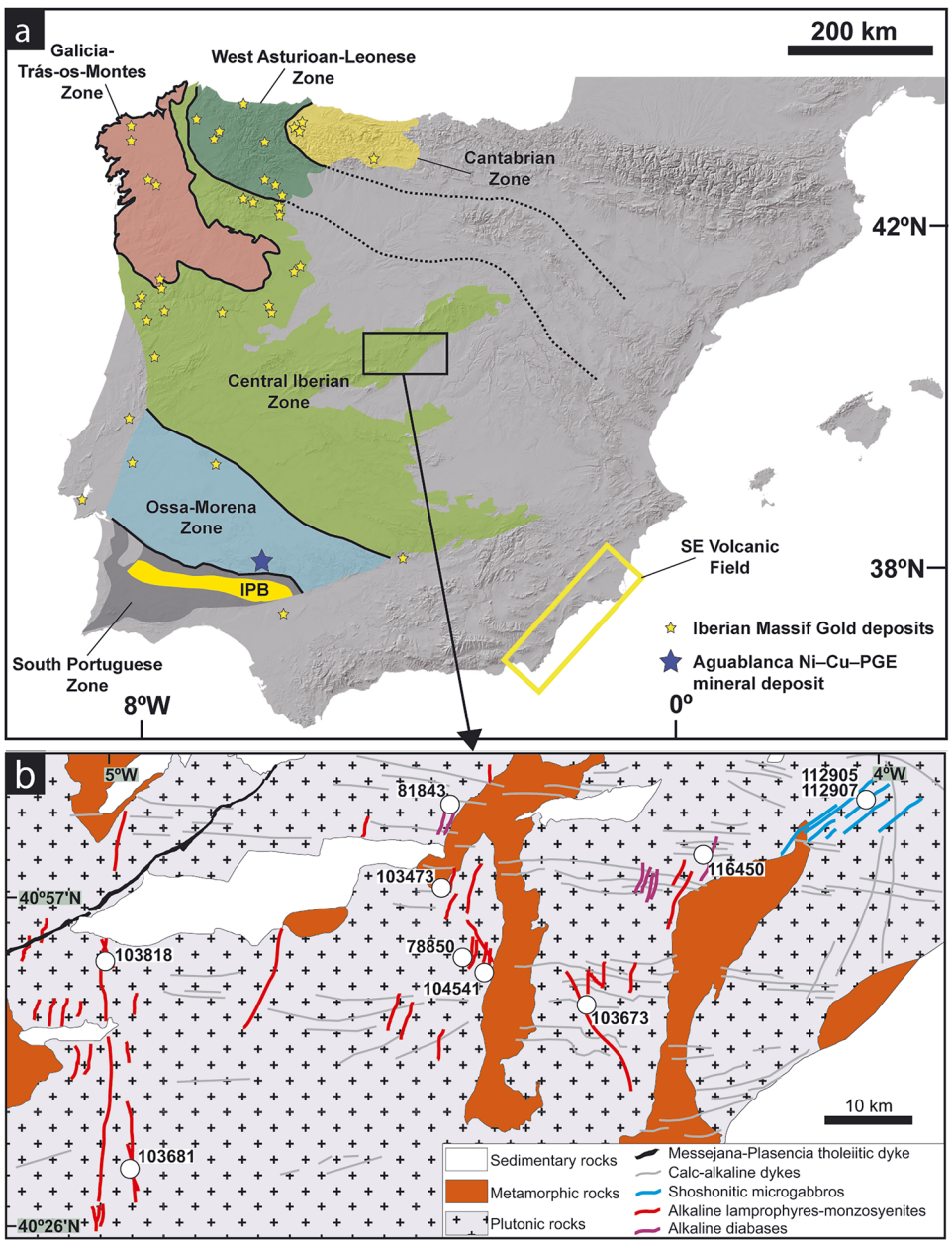

Fig. 1 **a** Zonation of the Iberian Massif and location of the main Au and PGE mineral deposits (modified after Romer and Kroner 2018). Gold deposits are represented in yellow: as stars, a wide band (IPB: Iberian Pyrite Belt) and a rectangle (the SE Volcanic Field). **b**: Schematic geological map of the Spanish Central System showing the Permian post-tectonic and post-orogenic dykes of shoshonitic microgabbros and alkaline lamprophyres and diabases. Sample location is shown as white circles together with the numbers of samples with PGE–Au whole-rock analyses

post-collisional magmatism of variable geochemical affinity in the Iberian Massif, including Permian mafic post-collisional shoshonitic and post-orogenic lamprophyric dykes derived from a heterogeneously metasomatized mantle (Orejana et al. 2008, 2020) (Fig. 1b). The nature of sulphides and the whole-rock PGE-Au contents in these magmas are still unknown. Our study is focused on the noble metal composition of such intrusions, which can help determine the mineralizing potential of the upper mantle under central Spain with respect to PGE and Au and allows proposing a tentative model for noble metal mantle enrichment in this region. The petrography and major element contents of magmatic sulphides in these alkaline rocks are also described, as these minerals most probably control the PGE distribution (e.g., Piña et al. 2013) and therefore their genesis is key to the discussion on regional primary sources of base and precious metal ores (e.g., Naldrett 2004 and references therein).

Geological setting

The Iberian Massif has been subdivided in several zones according to their stratigraphic, structural and petrologic characteristics (e.g., Martínez–Catalán 2012), with the Central Iberian Zone (CIZ) representing the innermost region (Fig. 1a). The CIZ is mainly composed of Neoproterozoic to Early Paleozoic metasedimentary rocks, Cambrian–Ordovician orthogneisses and Variscan felsic intrusions. These latter granitic bodies outcrop abundantly in the SCS mountain range, where a variety of mafic magmatic events have also been recorded, spanning from late Variscan to post orogenic rifting stages (e.g., Orejana et al. 2020; Villaseca et al. 2022). The Variscan mafic magmatism is restricted to small gabbroic–dioritic intrusions and dykes of calc-alkaline affinity (Orejana et al. 2009, 2020; Villaseca et al. 2022), coeval with the abundant felsic intrusions in the range ~ 316–294 Ma (e.g., Dias et al. 2002; Orejana et al. 2020; Bea et al. 2021 and references therein). This is followed by a short period of magmatic quiescence and the subsequent intrusion (~ 285 Ma; Orejana et al. 2020) of monzonitic microgabbroic dykes of shoshonitic affinity (Huertas and Villaseca 1994; Villaseca et al. 2004), which are restricted to a specific area within the SCS (Fig. 1b) and still can be related to the Variscan cycle. Both these and the calc-alkaline dykes share geochemical features characteristic of post-collisional magmatism, such as high LILE contents and Th/Yb ratios, low Ce/Pb values and negative Nb–Ta anomalies (e.g., Villaseca et al. 2022). Post-orogenic mafic–ultramafic alkaline dykes also crosscut the SCS mainly with a N–S strike (Fig. 1b). They have been subdivided into diabases, camptonitic lamprophyres and monzosyenitic porphyries based on petrographic and geochemical data (Orejana et al. 2008). Geochronological studies have yielded Permian intrusion ages in the range 274–264 Ma (Orejana et al. 2020 and references therein). The intrusion of the large gabbroic Messejana–Plasencia tholeiitic dyke (Fig. 1b), dated at 203 ± 2 Ma (Ar–Ar in biotite; Dunn et al. 1998), represents the last magmatic event recorded in the SCS and is linked to the opening of the Atlantic Ocean.

The geochemistry of the above SCS mantle-derived rocks reveals the involvement of enriched mantle sources of different characteristics during and after the Variscan continental collision (Orejana et al. 2008, 2009, 2020; Villaseca et al. 2022). Incompatible trace element contents and isotopic ratios (Sr–Nd–Hf) point to melting of a lithospheric mantle with a continental imprint in the case of the late-orogenic magmatism, which has also been identified in SCS pre-Variscan mafic rocks (Orejana et al. 2017). The introduction of such crustal component has been related either to oceanic subduction associated to the Cadomian continental margin or to crustal recycling during the Variscan collision (or both) (e.g., Orejana et al. 2020). On the contrary, the post-orogenic Permian alkaline dykes were extracted from deeper mantle sources metasomatized by melts/fluids ascending from the asthenosphere, which yield high LILE, REE and HFSE contents (and positive Nb–Ta anomalies). This mantle, which likely represents a transitional level between the deeper lithosphere and the asthenosphere, has proved to be somewhat heterogeneous, as reflected by the ocurrence of slightly different alkaline rock types (diabases and lamprophyres–monzosyenites) (Orejana et al. 2020).

The CIZ holds relevant mineral deposits which have been recognized and exploited since before Roman times, including widely distributed gold mineralizations (Fig. 1a). The CIZ gold deposits and those from other zones of the Iberian Massif have been classified in three main types (e.g., Romer and Kroner 2018, and references therein): 1) orogenic, 2) intrusion-related and 3) stratabound mineralizations. The orogenic gold deposits are hosted in Variscan shear-zones and were formed due to hydrothermal circulation during a subsequent reactivation of these structures. The mineralizations appear mainly in the form of quartz veins and are included in episyenites. The intrusion-related gold is spatially and genetically associated to small Variscan post-tectonic stocks of felsic to intermediate composition (granodiorites to monzodiorites), which promote intra- and extra-plutonic hydrothermal alteration and sulphide-Au precipitation (Romer and Kroner 2018). Stratabound gold appears either as paleo-placers or related to metal redistribution during the Variscan metamorphism of Cambro–Ordovician black shales and sandstones, giving rise to disseminated mineralizations and lithologically-controlled quartz veins. The proposed sources of these gold mineralizations are the massive sulphide deposits of SW Iberia (Iberian Pyrite Belt; South Portuguese Zone) and Cambrian to Ordovician metasedimentary layers deposited on the Cadomian basement (Romer and Kroner 2018).

PGE ore deposits are extremely rare in the Iberian Massif. Only one exceptional case has been documented:

the Aguablanca Ni–Cu–PGE sulphide deposit (Ossa-Morena Zone; SW Iberia) (Fig. 1a). This mineralization is associated to an Early Carboniferous mafic stock which is part of the calc-alkaline Santa Olalla Igneous Complex (e.g., Piña et al. 2008). Apart from its uniqueness in SW Europe, other uncommon features of this deposit are its placement in a subvertical magmatic breccia and its association with a convergent plate margin setting. The mineralization is interpreted as derived from a sulphide melt segregated from an evolving underlying magma chamber.

Analytical methods

Ten samples representative of the different types of mafic dykes in the study area were selected for petrographic analysis and whole-rock PGE and Au determinations. These samples have sizes in the range 10–15 cm in diameter and include: 6 alkaline lamprophyres, 2 alkaline diabases and 2 shoshonitic microgabbros. Polished thin sections and rock powders were prepared at the Mineralogy and Petrology Department Sample Preparation Facility (Complutense University of Madrid, Spain). The major element composition of sulphides has been obtained with a JEOL Superprobe JXA 8900-M electron microprobe (Centro Nacional de Microscopía Electrónica "Luis Bru", Complutense University of Madrid), equipped with four wavelength-dispersive mode spectrometers. The acceleration voltage was 20 kV and the beam current 50 nA. Counting times were 20 s on the peak and 10 s on each background position. The beam diameter ranged from 0 to 5 µm. Comparison with natural and synthetic reference materials (Galena, GaAs, CoNiCr alloy, Fe, Sb, Cd, Zn, Mo, Ni, Bi and Cu) allowed the determination of the absolute abundance of the following elements: Fe, S, Co, Ni, Mo, Cu, Zn, Cd, Pb, Bi, As and Sb. Detection limits for the analysed elements fall in the range 0.013–0.078 wt% and consider the average value plus 6 times the standard deviation. The ZAF program was used for data correction.

Whole-rock PGE and Au analyses were performed at the Geoscience Laboratories of the Ontario Geological Survey (Sudbury, Canada). The conventional nickel sulphide (NiS) fire-assay pre-concentration technique and the tellurium co-precipitation were employed before analyses by ICP-MS. Replicate analyses of the standards TDB-1, OREAS 681 y OREAS 13b, together with an in-house standard, were undertaken in order to assess analytical precision and accuracy. Detection limits for the elements analysed are: 0.025 ppb (Ir), 0.08 ppb (Ru), 0.05 ppb (Rh), 0.19 ppb (Pt), 0.2 ppb (Pd), 0.6 ppb (Au). Analytical error in these elements is in the range 1.5–14.3%.

Petrography

Alkaline lamprophyres and diabases

The lamprophyres and diabases are porphyritic (mostly 5–15 vol%), with the former displaying the higher phenocrysts abundance (occasionally up to ~ 40 vol%). Lamprophyres have been classified as camptonites (Orejana et al. 2008) and have only mafic phenocrysts such as clinopyroxene (diopside-augite), amphibole (kaersutite), phlogopite and oxides (ulvöspinel, Ti-magnetite, ilmenite), of variable size (from a few millimetres to several centimetres) (Fig. 2a, b). H_2O-bearing minerals (amphibole and phlogopite–biotite) are restricted to the groundmass in the diabases, but these dykes include plagioclase phenocrysts which can be cm-sized (Fig. 2c). Olivine and chromite phenocrysts have also been recognised in accessory amounts, both in lamprophyres and diabases, although olivine is usually transformed to Mg-rich chlorite. Phenocrysts may be transformed to secondary phases (mainly chlorite) and partially to totally corroded, and they usually display complex zoning patterns (normal and reverse) (Orejana et al. 2007). The groundmass can be microcrystalline to cryptocrystalline and displays a similar mineral composition to that of the phenocrysts, as well as plagioclase in the case of the diabases. A variable typology of ocellar structures (feldspar-, chlorite- or carbonate-rich), is present both in the lamprophyres and diabases. Apart from chlorite, other low-T phases which can be found in the groundmass are sericite, calcite, zeolites (analcite) and epidote. These minerals are sometimes secondary in origin and associated to transformation of early crystallising minerals, but they can also represent late-stage crystallization from the lamprophyric-diabasic magma, once the exsolution of low-T volatile-rich fluids is reached (Rock 1991; and references therein).

Two of the analysed samples stands out for several specific petrographic features: (1) lamprophyre 103,818 for containing up to ~ 40 vol% phenocrysts (Fig. 2b) and a variable modal amount of opaque phenocrysts, such as ulvöspinel, Ti-magnetite and sulphides (pyrite, chalcopyrite and pyrrhotite) (up to 2 vol%), and (2) diabase 116,450 for the inclusion of small fragments (1–7 mm) of highly altered pyrite-bearing ultramafic xenoliths (Fig. 2e, f), which resemble other SCS enclaves (mainly clinopyroxenites and hornblendites) interpreted as deep-seated mafic cumulates (Orejana et al. 2006; Orejana and Villaseca 2008). The main alteration products of the mafic phases are Mg-rich chlorite and talc. These enclaves display a modal composition equivalent to the phenocryst assemblage of the host alkaline rocks, including scarce olivine pseudomorphs. Xenocrysts (clinopyroxene, quartz, garnet) and other types of xenoliths (mainly lower crust granulites) can also be found in these alkaline dykes.

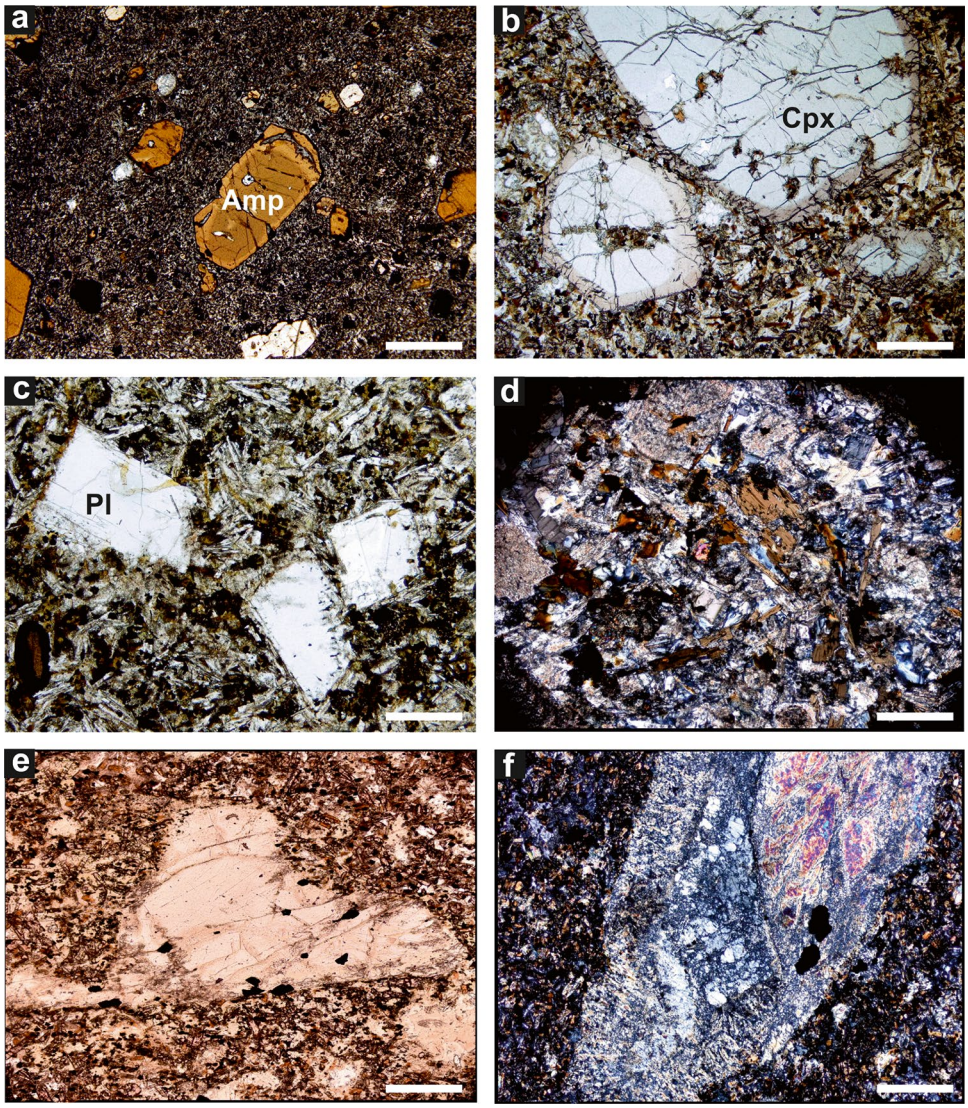

Fig. 2 Plane polarized (**a**, **b**, **c**, **e**) and cross polarized (**d**, **f**) light images showing the main petrographic textures of the studied mafic dykes. **a**: alkaline lamprophyre (103,473); **b**: alkaline lamprophyre (103,818); **c**: diabase (81,843); **d**: shoshonitic microgabbro (112,907); **e**–**f**: altered ultramafic xenoliths in diabase 116,450. The white bar represents 500 μm. Amp: amphibole; Cpx: clinopyroxene; Pl: plagioclase

Shoshonitic microgabbros

These dykes display porphyritic texture, with clinopyroxene (diopside-augite) and plagioclase (labradorite) phenocrysts up to ~ 0.5 cm in size, and a fine-grained holocrystalline groundmass including mainly these same phases, as well as biotite–phlogopite (Fig. 2d). The phenocrysts are euhedral to subhedral and variably altered to chlorite (cpx) and sericite (pl). The most common accessory minerals are ilmenite, apatite, magnetite, sulphides, zircon and titanite. The higher degree of alteration in some samples leads to formation of pseudomorphs with chlorite and calcite, which can also be present in the groundmass. Nonetheless, calcite can also be present as a primary magmatic mineral within ocelli or as an irregular interstitial phase. This suite of dykes also includes more evolved terms which may show quartz and K-feldspar, and amphibole (kaersutite) within the groundmass. Only the more mafic dykes were selected for the analytical work.

Sulphides petrography and chemistry

The sulphides recognised in the studied samples are pyrite, chalcopyrite, pyrrhotite and galena, pyrite being much more common than the rest. These sulphides are more abundant in the alkaline lamprophyres and diabases (which lack galena), whereas the shoshonitic microgabbros only display very small grains of chalcopyrite and galena, restricted to the groundmass. Pyrite crystals display a heterogeneous morphology (euhedral, subhedral and anhedral), sometimes forming clusters, and a size in the range 5–800 μm. According to petrography, pyrite can be classified in six groups: 1) within altered phenocrysts and cumulate xenoliths (Fig. 3a–c), 2) as inclusions within other phenocrysts (clinopyroxene, amphibole, apatite) (Fig. 3d–e), 3) as microphenocrysts (Fig. 3f), 4) in the groundmass (Fig. 3g), 5) surrounded by a Ti-magnetite rim (Fig. 3h), and 6) inside late-stage globular vesicles (Fig. 3i). Optical and back scattered electron (BSE) imaging do not

reveal any zoning in pyrites. Chalcopyrite appears mainly associated to pyrite in phenocrysts or in altered enclaves, always representing low proportions (Figs. 3a, f), and pyrrhotite is rare and only found as small globules (5–50 μm) included in phenocrysts (Fig. 3d).

Electron microprobe data of pyrite, chalcopyrite and pyrrhotite have been included in Table 1. Pyrite is characterised by a moderate heterogeneity in Fe (44.1–46.9 wt%) and S (51.9–54.7 wt%), with S/Fe atomic ratios in the range of 2.003–2.054. These values are always higher than the ideal stoichiometric ratio of 2, which implies that Fe is more readily substituted by base metals than S by As, Sb or other elements. Deviations from the mentioned stoichiometry are restricted to 0.14–2.69%, with the higher values being related to higher Ni contents.

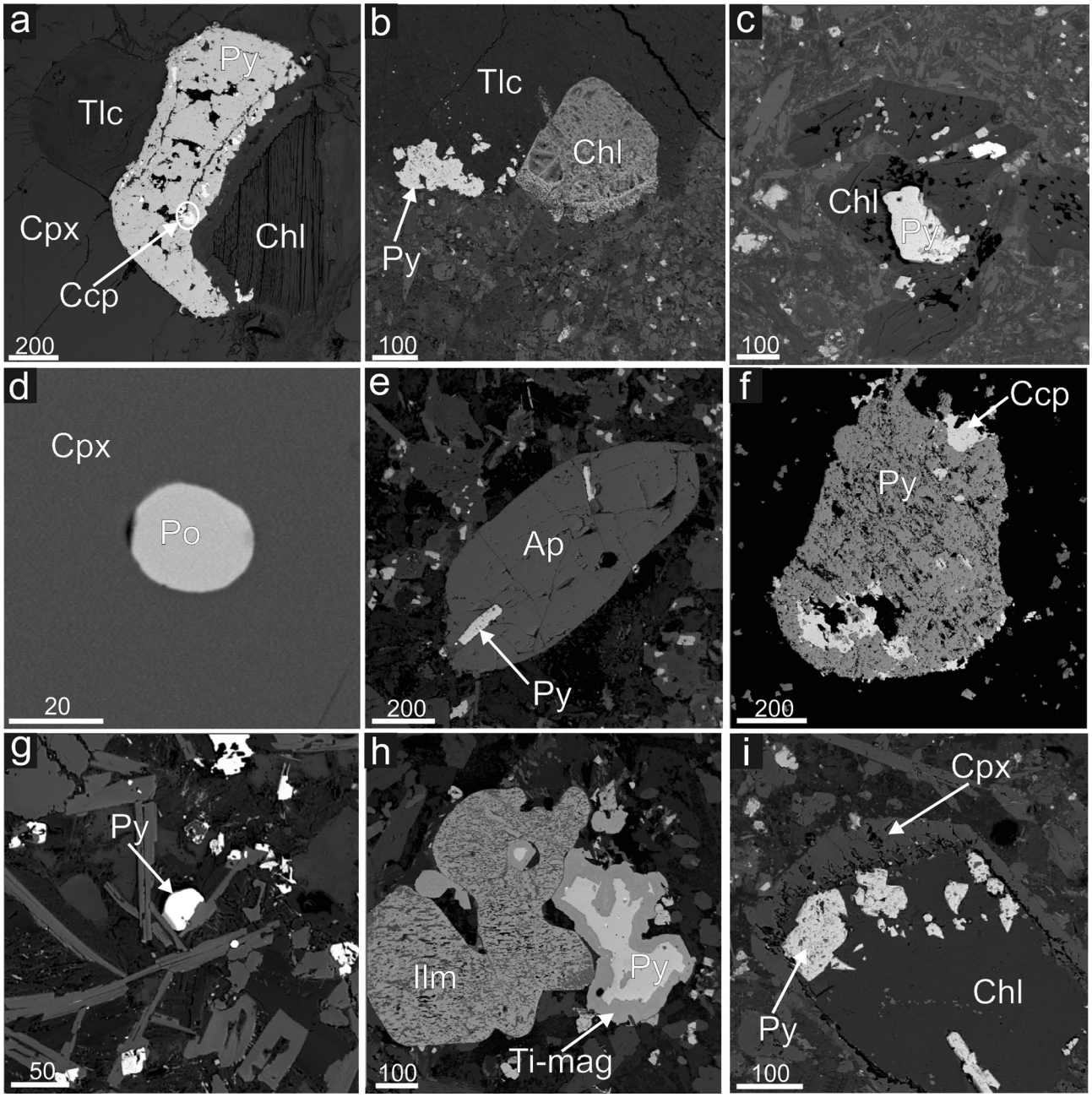

Fig. 3 Back scattered electron images of sulphides from the SCS mafic dykes. **a–c**: altered phenocrysts and mafic enclaves (samples 104,395, 116,450 and 103,673); **d**, **e**: inclusions in phenocrysts (samples 103,818 and 104,529); **f**: phenocrysts (sample 103657A); **g**: groundmass (sample 103,811); **h**: pyrite within Ti-magnetite (sample 103,817); **i**: low-T vesicle (sample 103657A). The number indicated in the scale bar at the bottom-left of each image represent size in microns. Py: pyrite, Ccp: chalcopyrite, Po: pyrrhotite, Ap: apatite, Cpx: clinopyroxene, Ilm: ilmenite, Mag: magnetite, Chl: chlorite, Tlc: talc

S and Fe concentrations are relatively homogeneous in the six pyrite groups (Fig. 4a, b). Pyrite clearly related to late-stage evolution (groundmass, pyrites in Ti-magnetite and vesicles) shows lower Ni values (sometimes below detection limit) when compared to pyrite inclusions and pyrite associated with altered xenoliths, which can reach values up to 1.16 wt% (Fig. 4c). Pyrite phenocrysts display Ni values similar to those of groundmass pyrites. Most base metal concentrations are close to or below detection limit (Table 1), and their homogeneous contents do not allow establishing significant differences between pyrite groups. It is remarkable that Cu and As show low values (Table 1), almost always below or very near the analytical detection limit.

Chalcopyrite, which is always associated to pyrite from altered enclaves and phenocrysts, shows a homogeneous composition, with S = 34.3–34.6 wt%, Fe = 29.7–30.4 wt% and Cu = 33.6–33.8 wt% (Table 1). The pyrrhotite inclusions do not show a significant compositional variation either (S = 39.28–39.89 wt%; Fe = 58.57–58.77 wt%), and their Ni concentrations only reach minor amounts (Ni = 0.27–0.31 wt%) (Table 1).

Noble and base metal geochemistry

PGE and Au contents determined in the present study are included in Table 2, together with Cu, Co and Ni concentrations previously obtained in the same samples (Orejana et al. 2008, 2020). Overall, the Ir, Rh and Ru contents are very low. Ir and Rh values are below detection limit in 8 out of 10 samples, ranging from 0.11 to 0.56 ppb and from 0.1 to 0.16 ppb, respectively, in lamprophyre 103,818 and diabase 116,450. Ru contents are also low, although above detection limit in all samples (0.08–0.93 ppb). The Pt, Pd and Au contents are significantly higher and more variable than the rest of PGE: Pt = 0.25–4.42 ppb; Pd = < 0.27–5.62 ppb and Au = 2–29 ppb. Ni, Co and Cu contents only reach moderate concentrations (Ni = 27–320 ppm; Co = 29–58 ppm; Cu = 21.6–70 ppm; Table 2).

When plotted against Mg# [Mg/(Mg + Fe^{2+})] (values taken from Orejana et al. 2008, 2020), an apparent positive correlation can be identified for Pd and Pt, as well as most base metals (Cr, Cu and Ni), whereas Au and IPGE do not show a clear tendency (Fig. 5; Ir and Rh have not been plotted due to the scarcity of data). It is noteworthy that the high Pd–Pt concentrations of sample 103,818 represent an anomaly with respect to the rest of lamprophyres, and the high base and noble metal values shown by sample 116,450, also fall out of any evolutionary trend. Considering the special petrographic features described in these two samples, this anomalous chemical composition is likely associated to higher relative modal proportions of sulphide minerals. Due to the distinct composition of these samples, not representative of primary melts, they have not been considered to further discuss the nature of the mantle sources and the metasomatic events.

The relative abundance of PGE and Au in the three dyke groups with respect to the Primitive Mantle values (McDonough and Sun 1995) is broadly similar and characterized by a marked fractionation between the Ir-group PGE (IPGE; Ir and Ru) and the Pd-group PGE (PPGE; Rh, Pt and Pd), the latter displaying much higher values (Fig. 6). The analytical detection limit values of Ir (0.025 ppb) and Rh (0.05 ppb) have been used to draw the thick dashed grey line in Fig. 6, which can be considered as an approximation to the likely maximum abundances of Ir and Rh in samples lacking Ir and Rh concentrations. The exceptions to the above general pattern are lamprophyre 103,818, which stands out due to its higher degree of enrichment in Pt and Pd, and diabase 116,450, which shows a flat Primitive Mantle-normalized pattern for most PGE (Fig. 6). Au shows a variable degree of enrichment in the normalized spectrum, giving rise to marked positive anomalies and abundances of 2–29 × Primitive Mantle. Co also shows a moderate positive anomaly, although its relative abundances are below 1 (Fig. 6). Cu abundance is lower than that of Au and its concentration is similar to that of the Primitive Mantle, except for sample 116,450 (diabase) which displays slightly higher values.

The above described low PGE contents contrast with the abundances shown by mafic rocks (kimberlites) from the Bastar craton (India), extracted from a PGE-enriched subcontinental mantle source (Chalapathi Rao et al. 2014) (Fig. 6). Other alkaline and calk-alkaline magmas derived from a similarly metasomatized mantle source also display slightly higher PGE values (Choi et al. 2020). These latter authors additionally document the occurrence of a variable, positive Au anomaly, which nevertheless does not reach the high abundances of our samples (Fig. 6).

Discussion

Nature of sulphides in the SCS mafic dykes

Sulphides in the SCS alkaline lamprophyres and diabases, although generally accessory, may reach significant modal amounts. Several features point to a magmatic origin: presence of pyrrhotite and pyrite inclusions within fresh primary phenocrysts (clinopyroxene, amphibole and apatite) (Fig. 3d, e), occurrence of disseminated pyrite (either as phenocrysts or in the groundmass) (Fig. 3f–g), coexistence with magmatic Ti-magnetite (Fig. 3h) and low values for most trace metals (e.g., Co, Cu, Zn, As, Sb, Pb and Bi; Table 1). Moreover, they do not show any textural evidence of alteration by hydrothermal fluids.

Models on the evolution of magmatic sulphides are based on experimental studies of ternary or quaternary systems involving Ni, Fe, Cu and S (Naldrett 2004, and

Table 1 Representative major and minor element composition of the main sulphides from the SCS mafic dykes

	LLD*	Pyrite																Chacopyrite		Pyrrhotite	
Sample		103657A			103811	103817		103673				104395	104529		116450		1036857A		104395	103818	
Analysis		1	2	5	8	11	14	23	24	25	27	17	19	20	4	3	4	6	16	34	35
*Type***		v	v	ph	ph	ph	gr	ph	inc	inc	inc	enc	inc	gr	enc	enc	ph	ph	enc	inc	inc
Fe	0.02	46.89	46.48	45.44	46.8	46.82	44.09	46.65	46.34	46.41	46.78	44.35	44.67	46.39	45.6	45.79	30.34	30.36	30.03	58.77	58.57
S	0.08	53.23	53.4	52.9	53.05	53.45	54.72	53.86	52.72	52.6	52.6	53.59	53.42	53.06	53.27	51.99	34.52	34.21	34.9	39.89	39.38
Cu	0.03	bdl	bdl	bdl	bdl	bdl	bdl	bdl	bdl	bdl	bdl	bdl	bdl	bdl	bdl	bdl	33.99	34.06	33.76	bdl	bdl
Ni	0.02	bdl	bdl	0.41	0.02	0.03	bdl	bdl	0.16	0.14	bdl	0.65	1.16	bdl	0.49	0.36	bdl	bdl	bdl	0.27	0.31
Mo	0.07	bdl	bdl	bdl	bdl	bdl	bdl	bdl	bdl	bdl	bdl	bdl	bdl	bdl	bdl	bdl	bdl	bdl	bdl	bdl	bdl
Pb	0.32	0.51	bdl	0.37	bdl	0.38	0.42	bdl	0.66	0.75	bdl	bdl	bdl	bdl	bdl	0.72	0.92	bdl	bdl	bdl	bdl
Bi	0.12	bdl	bdl	bdl	bdl	bdl	bdl	bdl	bdl	0.17	0.26	bdl	bdl	0.21	bdl	bdl	0.07	bdl	bdl	0.19	bdl
Co	0.01	0.07	0.08	0.06	0.05	0.06	0.08	0.08	0.04	0.08	0.08	0.06	0.09	0.05	0.1	0.08	0.03	0.04	0.02	0.11	0.08
Sb	0.03	0.03	bdl	0.04	bdl	0.03	bdl	0.03	0.03	0.03	bdl	bdl	bdl	0.03	0.04	bdl	bdl	bdl	0.03	0.06	0.04
As	0.03	0.04	0.04	bdl	bdl	0.03	0.06	bdl	0.03	bdl	0.07	bdl	bdl	0.05	0.03	0.04	bdl	bdl	bdl	0.04	0.03
Zn	0.02	bdl	bdl	bdl	bdl	bdl	bdl	bdl	bdl	bdl	bdl	bdl	bdl	bdl	bdl	bdl	0.04	0.03	0.02	bdl	bdl
Cd	0.02	0.000	bdl	bdl	0.02	0.02	bdl	0.02	0.02	bdl	0.04	0.03	bdl	bdl	bdl	0.02	0.04	bdl	bdl	0.02	0.04
Sn	0.02	bdl	bdl	bdl	bdl	bdl	0.02	bdl	0.02	bdl	bdl	bdl	bdl	bdl	bdl	0.02	0.03	bdl	bdl	bdl	bdl
Total		100.8	100	99.2	99.9	100.8	99.4	100.6	100	100.2	99.8	98.7	99.3	99.8	99.5	99	100	98.7	98.8	99.3	98.5
*atoms per formula unit****																					
Fe		0.995	0.998	0.988	0.997	0.996	0.995	0.996	0.992	0.99	0.996	0.984	0.973	0.998	0.988	0.986	0.501	0.502	0.502	6.951	6.953
S		1.999	1.999	1.999	2.000	1.999	1.999	2.000	1.999	2.000	1.999	2.000	1.999	1.999	1.999	1.999	2.000	1.999	1.999	7.994	7.995
Cu		0.000	0.000	0.000	0.000	0.000	0.000	0.000	0.000	0.000	0.000	0.000	0.000	0.000	0.000	0.000	0.493	0.495	0.496	0.000	0.000
Ni		0.000	0.000	0.008	0.000	0.001	0.000	0.000	0.003	0.003	0.000	0.014	0.024	0.000	0.01	0.007	0.000	0.000	0.000	0.031	0.035
Mo		0.000	0.000	0.000	0.000	0.000	0.000	0.000	0.000	0.000	0.000	0.000	0.000	0.000	0.000	0.000	0.000	0.000	0.000	0.000	0.000
Pb		0.003	0.000	0.002	0.001	0.002	0.003	0.002	0.004	0.004	0.000	0.001	0.001	0.000	0.000	0.004	0.004	0.001	0.001	0.000	0.001
Bi		0.000	0.000	0.000	0.000	0.000	0.000	0.000	0.000	0.001	0.002	0.000	0.000	0.001	0.000	0.000	0.000	0.000	0.000	0.006	0.000
Co		0.001	0.002	0.001	0.001	0.001	0.002	0.002	0.001	0.002	0.002	0.001	0.002	0.001	0.002	0.002	0.001	0.001	0.000	0.012	0.009
Sb		0.000	0.000	0.000	0.000	0.000	0.000	0.000	0.000	0.000	0.000	0.000	0.000	0.000	0.000	0.000	0.000	0.000	0.000	0.000	0.000
As		0.001	0.001	0.000	0.000	0.000	0.001	0.000	0.000	0.000	0.001	0.000	0.000	0.001	0.000	0.001	0.000	0.001	0.000	0.003	0.002
Zn		0.000	0.000	0.000	0.000	0.000	0.000	0.000	0.000	0.000	0.000	0.000	0.000	0.000	0.000	0.000	0.000	0.000	0.000	0.000	0.000
Cd		0.000	0.000	0.000	0.000	0.000	0.000	0.000	0.000	0.000	0.000	0.000	0.000	0.000	0.000	0.000	0.000	0.000	0.000	0.001	0.002
Sn		0.000	0.000	0.000	0.000	0.000	0.000	0.000	0.000	0.000	0.000	0.000	0.000	0.000	0.000	0.000	0.000	0.000	0.000	0.000	0.000
Total		3.000	3.000	3.000	3.000	3.000	3.000	3.000	3.000	3.000	3.000	3.000	3.000	3.000	3.000	3.000	3.000	3.000	3.000	15.00	15.00

BDL Below Detection Limit

*LLD Lower Limit of Detection (wt%)

**v: vesicles, ph: phenocrysts, gr: groundmass, enc: altered xenoliths, inc: inclusions

***stoichiometric formulae of sulphides: FeS_2 (pyrite), $CuFeS_2$ (chalcopyrite) and Fe_7S_8 (pyrrhotite)

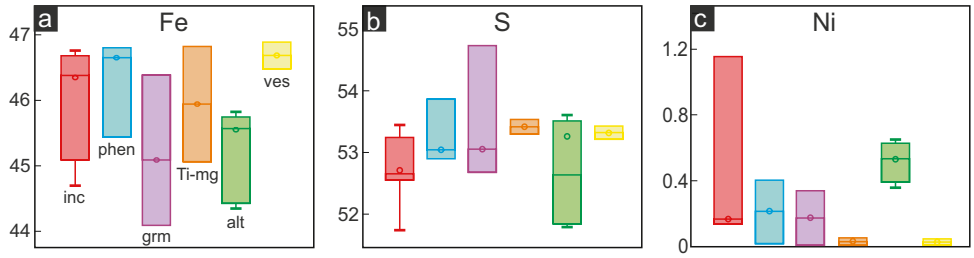

Fig. 4 Box plot displaying the Fe, S and Ni composition (wt%) of pyrites from the SCS alkaline dykes. The central box is the middle 50% of the data. The line and circle in each box represent the median and mean value, respectively. The key for each pyrite group is indicated in diagram a; inc: pyrite inclusions within fresh primary minerals (amphibole, clinopyroxene, apatite), phen: phenocrysts, grm: groundmass pyrite, Ti-mg: pyrite with rim of Ti-magnetite, alt: pyrite in altered enclaves or phenocrysts, ves: pyrite within vesicles

references therein). The absence of Ni-rich phases, such as pentlandite, in the studied SCS mafic dykes likely suggests that Ni could have been exhausted almost completely before sulphide exsolution, and the system Cu–Fe–S would be the most appropriate reference model. The experiments and observations of natural assemblages predict the formation of a Cu-rich (Ni-poor) intermediate solid solution (iss) from, or in conjunction with, a Fe-rich monosulphide solid solution (mss) (Jensen 1942; Kullerud et al. 1969; Naldrett 2004). The presence of pyrrhotite and pyrite inclusions in mafic phenocrysts implies that exsolution of such sulphide melt is not a late-stage process but happened during fractionation at depth. The scarce pyrrhotite globules found within mafic phenocrysts likely formed by exsolution from mss. On the other hand, pyrite inclusions and phenocrysts could derive from mss or iss (Naldrett et al. 1967; Naldrett 2004; Dare et al. 2011). The predominance of pyrite over pyrrhotite in the studied rocks is not a usual feature of sulphide melts segregated from most mafic magmas, but it is not rare in ultramafic–mafic volatile-rich alkaline rocks (Graham et al. 2017) akin to the SCS diabases and lamprophyres. Thus, pyrite inclusions and phenocrysts could be considered primary phases, and their preferred equilibration over pyrrhotite is likely related to relatively high fS_2 in the liquid. The broadly low Cu and Ni concentrations in pyrite and pyrrhotite (Table 1; Fig. 4c) (and scarcity of chalcopyrite) also suggest that this sulphide saturation was a relatively early process, as Ni is compatible during silicate liquid fractionation (Koshlyakova et al. 2022 and references therein).

The presence of pyrite within mafic–ultramafic cumulate xenoliths could in principle favour a primary origin during crystal settling. However, pyrite in these enclaves is only found in altered zones, mostly in their boundaries or where magma infiltration is apparent (Figs. 2e, f and 3b). Such feature, as well as the absence of reaction textures in the pyrite itself, calls for a second process of sulphur exsolution occurring during xenolith alteration. Mineral

Table 2 Noble and base metal composition of the SCS mafic dykes

	LLD*	Shoshonitic microgabbro		Alkaline lamprophyres						Alkaline diabases
Sample		112905	112907	78850	103473	103673	10368	103818	104541	116,450
Au (ppb)	0,6	21,5	11,7	7,0	7,6	2,0	6,6	10,9	22,6	29,0
Ir (ppb)	0,025	bdl	bdl	bdl	bdl	bdl	bdl	0,11	bdl	0,56
Pd (ppb)	0,2	0,27	0,80	0,30	bdl	0,38	bdl	5,62	0,63	1,62
Pt (ppb)	0,19	0,39	0,67	0,39	bdl	0,31	bdl	4,42	0,39	1,40
Rh (ppb)	0,05	bdl	bdl	bdl	bdl	bdl	bdl	0,10	bdl	0,16
Ru (ppb)	0,08	0,12	0,09	0,18	0,09	0,12	0,08	0,10	0,11	0,93
Cr (ppm)**	5,0	110	270	167	35,4	258	66,4	183	272	480
Cu (ppm)**	5,0	40,0	40,0	37,1	28,7	42,6	21,6	44,9	39,2	70,0
Co (ppm)**	0,3	29,0	29,0	34,5	34,1	41,2	31,5	36,2	34,4	58,0
Ni (ppm)	5,0	60,0	90,0	55,6	22,5	82,3	27,0	55,8	103	320

BDL Below Detection Limit

*LLD Lower Limits of Detection

**Cr, Cu, Co and Ni concentrations taken from Orejana et al. (2008, 2020)

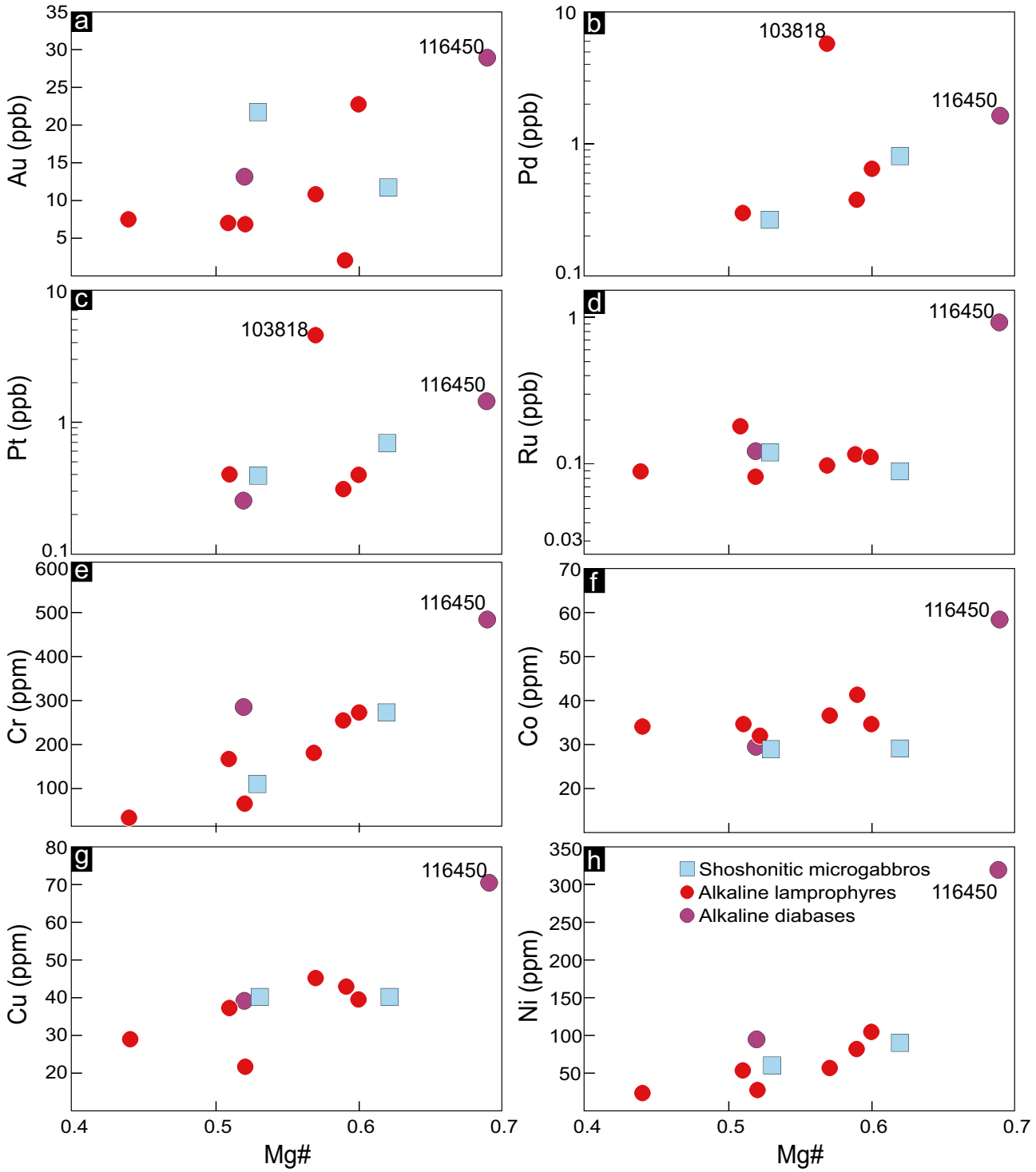

Fig. 5 Noble and base metal composition of the SCS mafic dykes plotted against Mg#. Samples 116,450 and 103,818 have been highlighted where they display a distinct composition with respect to other samples (see text for further explanation)

assemblages including chlorite, talc and pyrite, resulting from reaction of mafic–ultramafic rocks and hydrous fluids, have been described elsewhere (e.g., Smith 1995). The alkaline magma ascent, and its associated pressure decrease, could have provoked volatile exsolution (H_2O and CO_2), which promoted vesiculation and alteration of suspended solids (xenoliths and phenocrysts) (e.g., Rock 1991). The consumption of H_2O and CO_2, resulting in

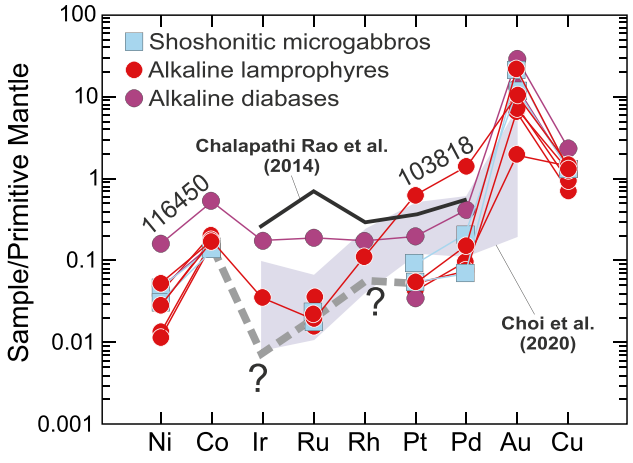

Fig. 6 Primitive Mantle-normalized abundances of noble and base metals in the SCS mafic dykes. Primitive Mantle values after McDonough and Sun (1995). Au–PGE composition of kimberlites from the Bastar craton (Chalapathi Rao et al. 2014) and calk-alkaline lamprophyres from the Yilgarn craton (Choi et al. 2020) have been plotted for comparison. Question marks in Ir and Rh indicate that the composition of these elements is below detection limit: the dashed line has been drawn considering these values and represents an estimated maximum composition

chlorite and talc formation during the xenoliths transformation, would reduce the oxygen fugacity, increase fS_2 and facilitate sulphide crystallization. Such reactions, leading to pyrite stabilization, have already been described in mafic rocks (e.g., Kanitpanyacharoen and Boudrau 2013; Piña et al. 2013). The late-stage volatile-rich (hydrothermal) fluids responsible for this autometasomatic transformation would also explain the formation of pyrite in the groundmass, included in vesicles and associated to altered mafic phenocrysts. Likewise, a late-stage process is consistent with pyrite crystals included in Ti-magnetite from sample 103,817 (Fig. 3h). Ti-magnetite is a late crystallizing mineral and its formation may cause redox changes in the melt (a decrease in oxygen fugacity), which in turn may trigger S saturation (e.g., Jenner et al. 2010). Chalcopyrite, which is scarce and associated to pyrite phenocrysts and pyrite formed during late-stage alteration, likely resulted from iss breaking down during cooling, as both chalcopyrite and pyrite can coexist in equilibrium at temperatures above 150 ºC (Naldrett 2004).

The two sulphur saturation processes mentioned above have not led to noticeable differences in pyrite composition, except for Ni. Pyrites from the groundmass, vesicles and inclusions in Ti-magnetite display undetectable or low Ni concentrations, when compared to pyrite inclusions in mafic minerals (Fig. 4c). The relatively high Ni contents of pyrite in altered mafic minerals (Fig. 4c) could be explained by a variable incorporation of these elements from the transformed mafic phases.

Evaluation of post-magmatic processes on PGE–Au geochemistry

There is evidence of post-magmatic transformation of the SCS shoshonitic and alkaline dykes, recorded in the form of low-T phases (chlorite, sericite, calcite, zeolites, epidote) which can be found mainly in the groundmass, in ocellar structures (vesicles) and within altered (pseudomorphosed) phenocrysts. Although circulation of hydrothermal fluids is commonly associated with shoshonitic and lamprophyric mafic magmatism (e.g., Müller and Groves 2019), much of the alteration found in these rocks is caused by metasomatism induced by the volatile-rich melt fraction remaining in the last stages of crystallization, typical of lamprophyric and related rocks (Rock 1991; Mitchell 1995). Whatever the origin, the question is to what extent such alteration processes may have affected the PGE and Au concentrations.

Wang et al. (2008) have suggested that hydrothermal fluids circulation may be responsible for PGE mobilization (and reprecipitation) at low temperatures. Taking into account that secondary minerals abundance in the studied rocks is broadly lower than 5 vol% (only some shoshonitic dykes show alteration up to 10–15%), any modification of their PGE composition due to such hydrothermal process seems to be negligible. In any case, the role played by alteration in the noble metals content can be tested using the Alteration Index (AI) of Ishikawa et al. (1976) $[[(K_2O+MgO)/(Na_2O+K_2O+CaO+MgO)]\times 100]$, and its potential correlation with PGE–Au. As shown in Fig. 7, there is no clear correlation between AI and Ru, Pt, Pd or Au, suggesting that noble metals were mostly immobile during alteration. This conclusion is reinforced by the positive slope of the Primitive Mantle-normalised pattern from Pt to Pd (Fig. 6), which is consistent with a magmatic context (Gan and Huang 2017). Flat patterns or those displaying negative slope could account for a relevant role of alteration, as Pd is the most mobile PGE (Barnes et al. 1985). Accordingly, the PGE–Au contents of the studied shoshonitic and alkaline dykes can be considered reliable indicators of the noble metal geochemical signature of the mantle sources underlying the Spanish Central System at the time of emplacement.

PGE abundance and behaviour

Several processes have been suggested to explain an IPGE–PPGE fractionation in mafic magmas such as that observed in our samples: fractionation of Ir–Ru alloys (Maier and Barnes 1999) or other early crystallizing minerals (e.g., Barnes and Picard 1993), low degrees of mantle partial melting (e.g., Lorand et al. 2008) and sulphide segregation (e.g., Amosse et al. 1990). The compatible behaviour of Os, Ir and Ru during mafic magma fractionation (Barnes et al. 1985) can give rise to small Os–Ir–Ru sulphide and alloy inclusions in high-temperature minerals, such as

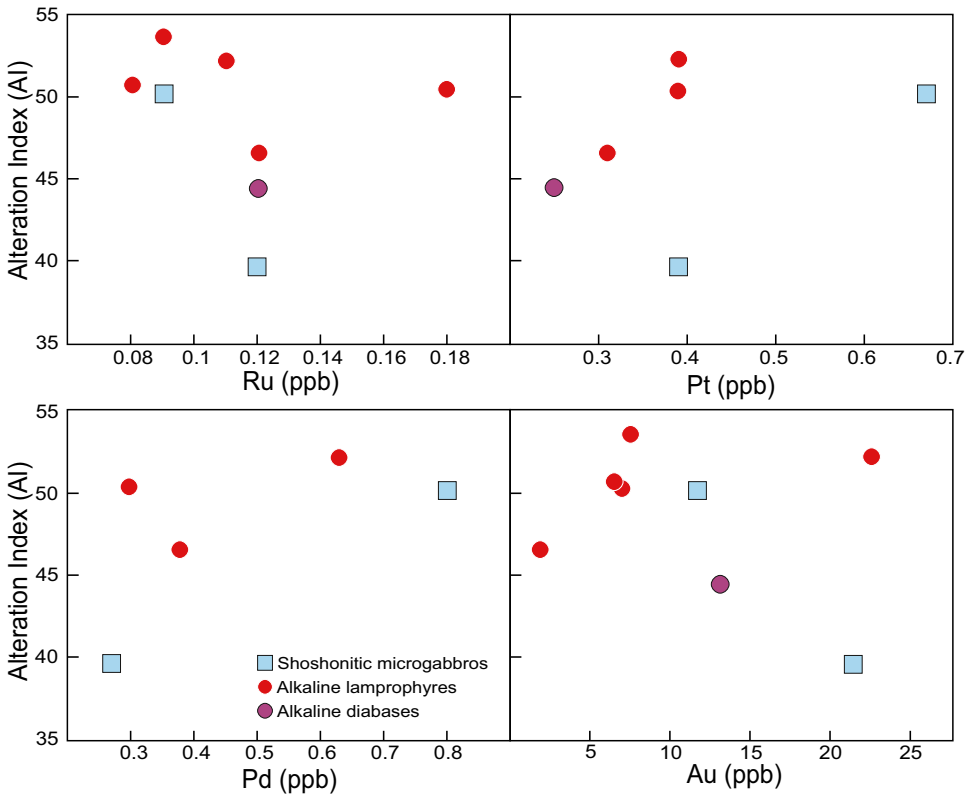

Fig. 7 Nobel metal (Au, Pt, Pd and Ru) concentrations vs. the Alteration Index (AI) of Ishikawa et al. (1976) [[(K2O + MgO)/(Na2O + K2O + CaO + MgO)] × 100] in the studied SCS mafic dykes

chromite and olivine (e.g., Zhou 1994). Ru exhibits a more compatible behaviour with Mg-rich phases than the rest of PGE and, therefore, it shows higher relative abundances in olivine (Dale et al. 2009). However, the lack of a negative Ru anomaly in the Primitive Mantle-normalized spectrum and of a positive correlation of Ru and Mg# of the studied rocks (Figs. 5d and 6), suggest that IPGE fractionation during deep-seated crystal fractionation did not played a key role in the PGE behaviour.

Low degree partial melting of sulphide-bearing mantle sources could also account for PGE fractionation, as these elements are mainly concentrated in Fe–Ni monosulphide phases and intergranular sulphides (e.g., pentlandite, chalcopyrite, isocubanite) (Lorand et al. 2008). This second group of sulphides is relatively enriched in PPGE with respect to IPGE and melts preferentially for low degrees of partial melting with respect to monosulphides, which are retained in the residual mantle (Ballhaus et al. 2006). Therefore, the low degrees of partial melting

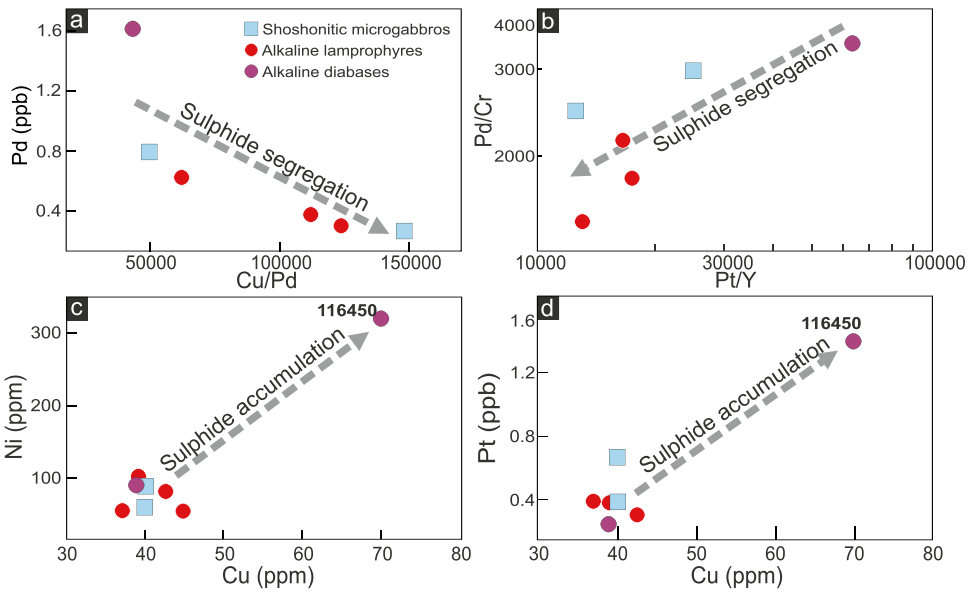

Fig. 8 Cu/Pd ratio vs. Pd (**a**), Pt/Y ratio vs. Pd/Cr ratio (**b**) and Cu vs. Ni and Pt (**c**, **d**) in the studied SCS mafic dykes

proposed for the studied rocks (1–2%; Villaseca et al. 2022) are in accordance with this possibility.

Alternatively, sulphur saturation in magmas and subsequent sulphide segregation could also account for the IPGE–PPGE fractionation due to the different partition coefficients of these elements (e.g., Barnes et al. 1985). Considering that S and Cu show a similar behaviour during magmatic differentiation, Cu can be considered a proxy for sulphur. Several geochemical fingerprints, such as a negative correlation of Cu/Pd ratio and Pd concentration and a positive correlation of the Pd/Cr and Pt/Y ratios (Gan and Huang 2017), could be related to an early sulphide saturation and segregation, which would lead to a progressive decrease of Pt–Pd with respect to Cr–Y–Cu. This correspondence can be observed in the SCS mafic dykes (Fig. 8a, b) and points to an early crystallization of sulphides, which could also explain the positive correlation of Mg# with respect to Cu, Pt and Pd (Fig. 5). The fact that Cr and Ni also decrease towards lower Mg#, suggests that both mafic silicates fractionation and sulphide segregation justify the geochemical variability observed in the SCS mafic dykes. The presence of sulphides as inclusions within mafic phenocrysts in the alkaline lamprophyres and diabases supports this possibility.

The anomalous composition of diabase 116,450, which shows the highest IPGE values (Figs. 5 and 6), is likely related to the inclusion of highly altered pyrite-bearing ultramafic xenoliths. These enclaves are deep-seated cumulate xenoliths genetically related with the SCS lamprophyric and diabasic melts (Orejana et al. 2006; Orejana and Villaseca 2008). The reaction of these cumulates with the volatile-rich magma leads to formation of relatively abundant pyrite (as explained above), which can incorporate important IPGE and Rh amounts substituting Fe in its structure (Duran et al. 2015; Piña et al. 2013). The higher Ni, Cu, Co and Au contents of this sample compared to the rest of analysed rocks (Fig. 5a, f–h, Fig. 8c–d and Table 2) reinforces this idea and highlights the control exerted by sulphides on all chalcophile elements during magma fractionation. Similarly, the excessive Pt–Pd enrichment in lamprophyre 103,818 (Figs. 5b, c and 6) is probably associated with its petrographic characteristics. The abundance of phenocrysts in this sample (~35–40 vol.%), including pyrite, implies certain degree of crystal accumulation. The relative PPGE enrichment of the primary lamprophyric melt, together with the strongly compatible behaviour of Pt–Pd with late-stage crystallizing sulphides, can explain the anomalously high concentrations of these elements in this sample.

In summary, both early sulphur segregation and low degrees of mantle partial melting can justify the general pattern of PGE fractionation and the low PGE contents observed in the studied samples.

Gold abundance and behaviour

Au, Pt and Pd are chalcophile during magmatic processes. However, the gold enrichment shown by the SCS alkaline and shoshonitic dykes (concentrations 2–29 times higher than that of the Primitive Mantle) is much higher with respect to that of Pt and Pd (Fig. 6). These data suggest that one or more enrichment processes have occurred in the mantle source and that these processes have been more efficient for Au than for PGE.

The metasomatized lithospheric mantle is generally enriched in gold with respect to the primordial mantle, and the source of this gold is usually associated with fluids or melts derived from the descending plate in a subduction context (e.g., Groves et al. 2020), or to alkaline melts ascending from a mantle plume (e.g., Webber et al. 2012; Tassara et al. 2017). The SCS post-tectonic and post-orogenic shoshonitic and alkaline mafic dykes display highly incompatible trace element concentrations indicative of mantle metasomatism by infiltration of agents of contrasting nature: deep asthenospheric magmas for the alkaline lamprophyre sources and a subduction-derived metasomatic agent for the shoshonitic microgabbros (Orejana et al. 2020; Villaseca et al. 2022). Each of these two possibilities would produce different geochemical fingerprints in the partial melts. High La/Sm ratios imply the existence of a broad trace element enrichment, whereas high Th/Yb ratios support subduction and recycling of continental components in the mantle; on the other hand, high Nb/Yb ratios are consistent with metasomatism caused by magmas coming from the deep asthenospheric mantle, without evident crustal influence (e.g., Wilson 1989). Moreover, a Co positive anomaly (with respect to Ni and Ir) could be associated to subduction-related metasomatism (Holwell et al. 2019). An overall positive correlation exists in the analysed samples between Au and La/Sm (Fig. 9a). However, the alkaline lamprophyres and the shoshonitic microgabbros exhibit contrasting features with respect to Th/Yb and Nb/Yb ratios, with the lamprophyres displaying lower Th/Yb and higher Nb/Yb ratios with respect to the shoshonitic dykes (Fig. 9b, c). Moreover, the Th/Yb ratios display a broad positive correlation with respect to Au contents, whereas no clear connection seems to exist between Au and the Nb/Yb values.

The above data suggest that Au enrichment in the subcontinental lithospheric mantle under central Spain was mainly controlled by subduction processes, which are more efficient regarding Au enrichment than infiltration and reaction with alkaline melts coming from the convecting mantle. The fact that all samples yield Au and Co positive anomalies, including the alkaline lamprophyres and diabases (Fig. 6), might indicate that the metasomatism related to entrainment of deep magmas overprinted an older subduction-related metasomatic event (Fig. 10). The high $(Au/Cu)_N$ ratios (1.4–17.3; Table 2), reflected in the Au peak shown in Fig. 6, mean a higher addition of Au relative to Cu, a feature which could not be ascribed only to entrainment of sulphide-saturated melts. Although very high $(Au/Cu)_N$ values (~80–375) have

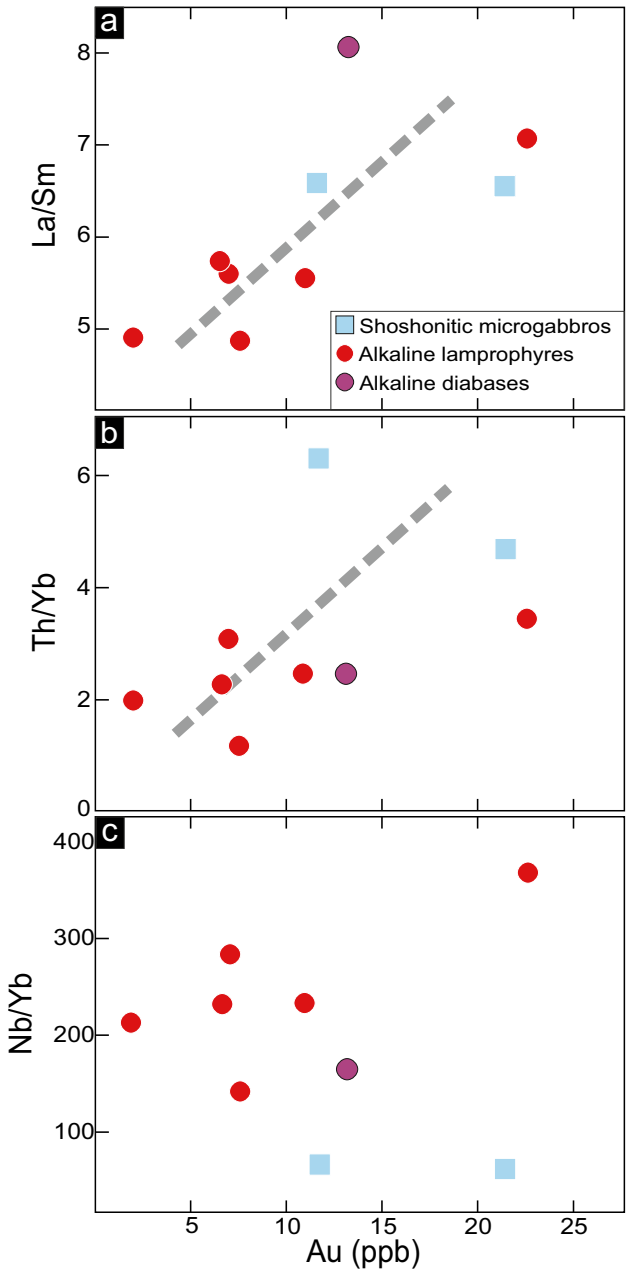

Fig. 9 La/Sm, Th/Yb and Nb/Yb ratios vs. Au contents in the studied SCS mafic dykes. The dashed line represents the broad correlation between Au concentrations and La/Sm and Th/Yb ratios. La/Sm, Th/Yb and Nb/Yb ratios have been calculated considering the data of Orejana et al. (2008, 2020)

been related to a secondary hydrothermal alteration of the mafic rock in the vicinity of Au mineralizations (Müller and Groves 2019, and references therein), this possibility is unlikely in the case of the SCS shoshonitic and alkaline mafic dykes, as they are fresh, yield much lower $(Au/Cu)_N$ ratios and are far from Au mineralizations. Alternatively, stronger Au enrichment in the mantle, relative to Cu, may be expected due to infiltration of S-rich fluids, as gold is more compatible with this hydrous phase than Cu (Pokrovski et al. 2014). This is in accordance with recent studies that emphasize the presence of restricted mantle domains with high heterogeneity, sometimes associated with variable reactive melt/rock ratios (Wang et al. 2022, and references therein), and suggests that the Au–Cu relative abundances shown by the SCS dykes are a characteristic inherited from their mantle source.

Noble metal fertility of the subcontinental lithospheric mantle under central Spain

The results presented above point to the presence of an Au-enriched mantle under central Spain, but the same is doubtful for the PGE. Even though alkaline-carbonatitic melts from the asthenosphere can be responsible for PGE enrichment in the lithospheric mantle (e.g., Alard et al. 2011; Akizawa et al. 2017), these elements always display subchondritic concentrations, most of them 10 to 100 times lower than chondrite (Fig. 6). The study of González-Jiménez et al. (2014) on mantle xenoliths from central Spain describes a Fe–Ni monosulphide solid solution with low PGE concentrations, interpreted as a residual phase after partial melting. No sign of PGE refertilization has been found in these mantle xenoliths. It is thus not surprising that PGE deposits are a rarity in the Iberian Massif, with only one exceptional example found in the Ossa-Morena Zone (the Aguablanca Ni–Cu–(PGE) sulphide deposit), where assimilation of sulphide-rich metasediments seems to have played a relevant role (Piña et al. 2008).

Most recent models highlight that Au endowment in certain metallogenic provinces is related to enrichment by fluids derived from a subducting oceanic plate (e.g., Holwell et al. 2019; Groves et al. 2020), whereas few examples have been explained as linked with continental subduction (Deng et al. 2020). The mantle under central Spain has been likely subjected to several enrichment events, including the Neoproterozoic oceanic subduction under the northern Gondwana margin (the Cadomian continental arc) and recycling of continental components during the Variscan continental collision (Orejana et al. 2020; Villaseca et al. 2022) (Fig. 10). Although both geodynamic contexts could be advocated for Au enrichment under the Central Iberian Zone, it is likely that oceanic subduction might have left a more significant imprint due to its longer lifespan and widespread extension.

Contrary to the PGE, gold deposits are relatively abundant in the Iberian Massif (e.g., Romer and Kroner 2018) (Fig. 1a). These authors summarize the main features of Paleozoic gold in the Variscides and establish three main types of gold deposits in Iberia (orogenic, intrusion-related and stratabound) associated to two auriferous sources: massive sulphide deposits of the Iberian Pyrite Belt and Cambrian–Ordovician siliciclastic sediments deposited on the

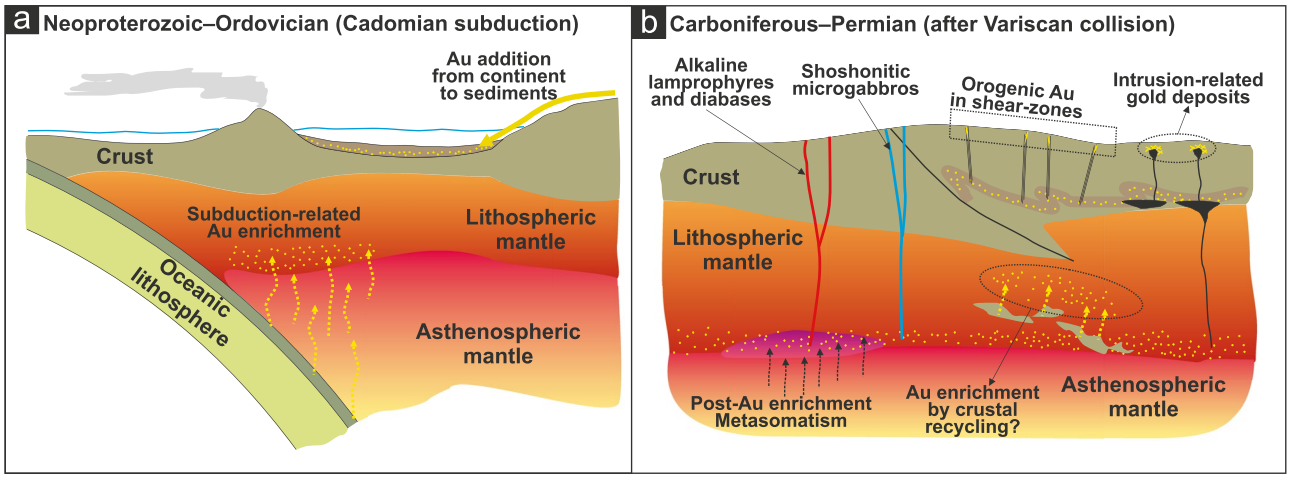

Fig. 10 Cartoon illustrating the geodynamic setting of gold enrichment under the Central Iberian Zone and generation of post-tectonic and post-orogenic mafic dykes, either during the Cadomian subduction (**A**) or late- to post-Variscan stages (**B**). The possible origin of orogenic and intrusion-related gold deposits in the CIZ is also represented in diagram B

Cadomian basement. Mobilization of gold contained in the volcanic massive sulphide deposits and in sediments with anomalous Au quantities during the low or medium grade Variscan metamorphism would be the main form of gold transfer and concentration to eventually yield gold deposits in the crust (Romer and Kroner 2018) (Fig. 10b).

However, the Au abundances shown by the mafic dykes analysed in this study highlight that the lithospheric mantle under central Spain should be considered another potential source of gold. It has been noted that potassic and shoshonitic igneous rocks (including alkaline lamprophyres) may coexist spatially and temporally with important orogenic and intrusion-related gold deposits (Rock and Groves 1988), although this association does not always imply the existence of a genetic link (e.g., Müller and Groves 2019). Accordingly, our data can be meaningful only regarding the study of the lithospheric mantle as a potential source of noble metal ores. In this sense, it is remarkable that the studied mafic dykes contain Au concentrations (2–29 ppb) higher than those of equivalent calc-alkaline and ultramafic lamprophyres (Au = 0.4–13.81 ppb) outcropping in areas with relevant gold deposits, such as the Yilgarn craton in Australia (Choi et al. 2020) (Fig. 6). These data indicate the relevance of the subcontinental lithospheric mantle under central Spain as a potential source of gold deposits. This kind of connection has already been proposed in SE Spain, where metasomatic Au-rich base-metal sulphides included in peridotite xenoliths have been considered the main metal source of the Miocene middle- to high-K calc-alkaline volcanism and, eventually, of the associated crustal gold mineralizations (Schettino et al. 2022). Such contribution of the metasomatized lithospheric mantle as a source of gold endowment in the upper crust has also been highlighted in previous studies (e.g., Tassara et al. 2017; Holwell et al. 2019; Wang et al. 2020).

Most gold deposits in the Central Iberian Zone seem to involve Au-bearing Cambrian–Ordovician metasediments. Such sources imply gold provenance from emerged neighbouring regions of the West-Gondwana Orogen (Romer and Kroner 2018) (Fig. 10a). However, a direct relation of the Iberian gold deposits with the underlying mantle is still possible in the case of intrusion-related deposits, as some Variscan stocks are associated to calc-alkaline mantle-derived magmas, including gabbroic–dioritic–monzonitic terms (e.g., Cuesta et al. 1998; Crespo et al. 2000; Martín-Izard et al. 2000) (Fig. 10b).

Conclusions

Pyrite and chalcopyrite are the main sulphides in the SCS post-collisional and post-orogenic mafic dykes and formed due to sulphur saturation in two distinct stages: an early stage characterised by crystal fractionation at depth, and a second and late stage related to magma ascent, CO_2 and H_2O exsolution, vesiculation, Ti-magnetite crystallization and cumulates alteration.

The PGE contents are generally low and fractionated from very low IPGE to moderate PPGE. These features seem to be associated to very low degrees of partial melting in the mantle sources and sulphide segregation at depth.

All analysed samples display moderate to high gold enrichment, comparable with equivalent mafic rocks extracted from other lithospheric mantle sections under gold-endowed provinces. The geochemistry of the SCS samples favour a subduction-related metasomatic event as the most likely geodynamic context for Au refertilization in the mantle.

The gold abundances shown by the mafic dykes analysed in this study highlight that the lithospheric mantle under central Spain should be considered a potential source of gold, as already pointed out for the mantle under SE Spain.

Acknowledgements We are grateful to Xabier Arroyo for his assistance during the petrographic characterization and to Alfredo Fernández Larios during the electron microprobe analyses. The constructive revision of two anonymous reviewers are highly acknowledged and have helped to improve the quality of the initial manuscript. This work is included in the objectives of, and supported by, the PID2020-115980GB-I00 project of the Ministerio de Educación y Ciencia of Spain.

Funding Open Access funding provided thanks to the CRUE-CSIC agreement with Springer Nature.

Reference

Akizawa N, Miyake A, Ishikawa A, Tamura A, Terada Y, Uesugi K, Takeuchi A, Arai S, Tanaka C, Igami Y, Suzuki K, Kogiso T (2017) Metasomatic PGE mobilization by carbonatitic melt in the mantle: Evidence from sub-μm-scale sulphide–carbonaceous glass inclusion in Tahitian harzburgite xenolith. Chem Geol 475:87–104

Alard O, Lorand JP, Reisberg L, Bodinier JL, Dautria JM, O'Reilly SY (2011) Volatile-rich metasomatism in montferrier xenoliths (Southern France): Implications for the abundances of chalcophile and highly siderophile elements in the subcontinental mantle. J Petrol 52:2009–2045

Amosse J, Allibert M, Fischer W, Piboule M (1990) Experimental study of the solubility of platinum and iridium in basic silicate melts – implications for the differentiation of platinum-group elements during magmatic processes. Chem Geol 81:45–53

Ballhaus C, Bockrath C, Wohlgemuth-Ueberwasser C, Laurenz V, Berndt J (2006) Fractionation of the noble metals by physical processes. Contrib Miner Petrol 152:667–684

Barnes SJ, Picard CP (1993) The behaviour of platinum-group elements during partial melting, crystal fractionation, and sulphide segregation: an example from the Cape Smith Fold Belt, northern Quebec. Geochim Cosmochim Acta 57:79–88

Barnes SJ, Naldrett AJ, Gorton MP (1985) The origin of the fractionation of the platinum-group elements in terrestrial magmas. Chem Geol 53:303–323

Barnes SJ, Anderson J, Smith T, Bagas L (2008) The Mordor Alkaline Igneous Complex, Central Australia: PGE-enriched disseminated sulphide layers in cumulates from a lamprophyric magma. Miner Deposita 43:641–662

Bea F, Gallastegui G, Montero P, Molina JF, Scarrow J, Cuesta A, González-Menéndez L (2021) Contrasting high-Mg, high-K rocks in Central Iberia: the appinite-vaugnerite conundrum and their (non-existent) relation with arc magmatism. J Iber Geol 47:235–261

Chalapathi Rao NV, Lehmann B, Balaram V (2014) Platinum-group element (PGE) geochemistry of Deccan orangeites, Bastar craton, central India: Implication for a non-terrestrial origin for iridium enrichment at the K-Pg boundary. J Asian Earth Sci 84:24–33

Choi E, Fiorentini M, Hughes H, Giuliani A (2020) Platinum-group element and Au geochemistry of Late Archean to Proterozoic calc-alkaline and alkaline magmas in the Yilgarn Craton. Western Australia Lithos 374–375:105716

Crespo JL, Moro MC, Fadón O, Cabrera R, Fernández A (2000) The Salamón gold deposit (León, Spain). J Geochem Explor 71:191–208

Cuesta A, Suárez O, Gallastegui G (1998) Caracterización geoquímica del magmatismo tardío en la Cordillera Cantábrica. Boletín Geológico y Minero De España 21:70–72

Dale CW, Burton KW, Pearson DG, Gannoun A, Alard O, Argles TW, Parkinson IJ (2009) Highly siderophile element behaviour accompanying subduction of oceanic crust: whole rock and mineral-scale insights from a high-pressure terrain. Geochim Cosmochim Acta 73:1394–1416

Dare SAS, Barnes SJ, Prichard HM, Fisher PC (2011) Chalcophile and platinum-group element (PGE) concentrations in the sulfide minerals from the McCreedy East deposit, Sudbury, Canada, and the origin of PGE in pyrite. Miner Deposita 46:381–407

Deng J, Wang Q, Santosh M, Liu S, Liang Y, Yang L, Zhao R, Yang L (2020) Remobilization of metasomatized mantle lithosphere: a new model for the Jiaodong gold province, eastern China. Miner Deposita 55:257–274

Dias G, Simoes PP, Ferreira N, Leterrier J (2002) Mantle and crustal sources in the genesis of late-Hercynian granitoids (NW Portugal): Geochemical and Sr-Nd isotopic constraints. Gondwana Res 2:287–305

Dunn AM, Reynolds PH, Clarke DB, Ugidos JM (1998) A comparison of the age and composition of the Sherburne Dyke, Nova Scotia, and the Messejana Dyke, Spain. Canadian JOURNAL Earth Sci 35:1110–1115

Duran C, Barnes SJ, Corkery JT (2015) Chalcophile and platinum-group element distribution in pyrites from the sulphide-rich pods of the Lac des Iles Pd deposits, Western Ontario, Canada: Implications for post-cumulus re-equilibration of the ore and the use of pyrite compositions in exploration. J Geochem Explor 158:223–242

Frimmel HE (2008) Earth's continental crustal gold endowment. Earth Planet Sci Lett 267:45–55

Gan T, Huang Z (2017) Platinum-group element and Re-Os geochemistry of lamprophyres in the Zhenyuan gold deposit, Yunnan Province, China: Implications for petrogenesis and mantle evolution. Lithos 283:228–239

González-Jiménez J, Villaseca C, Griffin W, O'Reilly S, Belousova E, Ancochea E, Pearson N (2014) Significance of ancient sulphide PGE and Re–Os signatures in the mantle beneath Calatrava, Central Spain. Contrib Miner Petrol 168:1–24

Graham SD, Holwell DA, McDonald I, Jenkin GRT, Hill NJ, Boyce AJ, Smith J, Sangster C (2017) Magmatic Cu-Ni-PGE-Au sulphide mineralisation in alkaline igneous systems: An example from the Sron Garbh intrusion, Tyndrum, Scotland. Ore Geol Rev 80:961–984

Groves DI, Santosh M, Deng J, Wang QF, Yang LQ, Zhang L (2020) A holistic model for the origin of orogenic gold deposits and its implications for exploration. Miner Deposita 55:275–292

Heidari SM, Daliran F, Paquette JL, Gasquet D (2015) Geology, timing, and genesis of the high sulphidation Au (–Cu) deposit of Touzlar, NW Iran. Ore Geol Rev 65:460–486

Holwell D, Fiorentini M, Mcdonald I, Lu Y, Giuliani A, Smith D, Keith M, Locmelis M (2019) A metasomatized lithospheric

mantle control on the metallogenic signature of post-subduction magmatism. Nat Commun 10:3511
Hronsky JMA, Groves DI, Loucks RR, Begg GC (2012) A unified model for gold mineralisation in accretionary orogens and implications for regional-scale exploration targeting methods. Miner Deposita 47:339–358
Huertas MJ, Villaseca C (1994) Les deniers cycles magmatiques posthercyniens du système central espagnol: les essaims filoniens calco-alcalins. Schweiz Mineral Petrogr Mitt 74:383–401
Ishikawa Y, Sawaguchi T, Iwaya S, Horiuchi M (1976) Delineation of prospecting targets for Kuroko deposits based on modes of volcanism of underlying dacite and alteration halos. Mining Geoloogy 26:105–117
Jenner FE, O'Neill HSC, Arculus RJ, Mavrogenes JA (2010) The magnetite crisis in the evolution of arc-related magmas and the initial concentrations of Au, Ag, and Cu. Journal of Petrolgy 51:2445–2464
Jensen E (1942) Pyrrhotite: melting relations and composition. Am J Sci 240:695–709
Kanitpanyacharoen W, Boudreau AE (2013) Sulfide-associated mineral assemblages in the Bushveld Complex, South Africa: platinum-group element enrichment by vapor refining by chloride-carbonate fluids. Miner Deposita 48:193–210
Kinnaird JA, Hutchinson D, Schürmann L, Nex PAM, de Lange R (2005) Petrology and mineralisation of the southern Platreef: northern limb of the Bushveld Complex, South Africa. Miner Deposita 40:576–597
Koshlyakova AN, Sobolev AV, Krasheninnikov SP, Batanova VG, Borisov AA (2022) Ni partitioning between olivine and highly alkaline melts: An experimental study. Chem Geol 587:120615
Kullerud G, Yund RA, Moh GH (1969) Phase relation in the Cu-Fe-Ni, Cu-Ni-S and Fe-Ni-S systems. Econ Geol 4:323–343
Lorand J-P, Luguet A, Alard O (2008) A New Set of Key Tracers for the Earth's Interior. Elements 4:247–325
Maier WD, Barnes SJ (1999) Platinum-group elements in silicate rocks of the lower, critical and main zones at union section western Bushveld Complex. J Petrol 40:1647–1671
Maier WD, Barnes S-J, Gartz V, Andrews G (2003) Pt-Pd reefs in magnetitites of the Stella layered intrusion, South Africa: A world of new exploration possibilities for platinum group elements. Geology 31:885–888
Martín-Izard A, Fuertes-Fuente M, Cepedal A, Moreiras D, García-Nieto J, Maldonado C, Pevida LR (2000) The Río Narcea Gold Belt intrusions: geology, petrology, geochemistry and timing. J Geochem Explor 71:103–117
Martínez-Catalán JR (2012) The Central Iberian arc, an orocline centered in theIberian Massif and some implications for the Variscan belt. Int J Earth Sci 101:1299–1314
McDonough WF, Sun SS (1995) The composition of the Earth. Chem Geol 120:223–253
Mitchell RH (1995) Kimberlites, Orangeites, and related rocks. Plenum Press, Nueva York, p 410
Müller D, Groves DI (2019) Potassic igneous rocks and associated gold-copper mineralization (fifth edition). Springer, Switzerland, p 398
Mungall JE (2002) Kinetic controls on the partitioning of trace elements between silicate and sulfide liquids. J Petrol 43:749–768
Mungall JE (2007) Magmatic ore deposits. In: Rudnick R (ed) The Crust. Treatise on Geochemistry Volume 3, Chapter 21. Elsevier, 1–33
Mungall JE, Naldrett AJ (2008) Ore deposits of the Platinum-Group Elements. Elements 4:253–258
Mungall JE, Brenan JM (2014) Partitioning of platinum-group elements and Au between sulfide liquid and basalt and the origins of mantle-crust fractionation of the chalcophile elements. Geochim Cosmochim Acta 125:265–289
Naldrett AJ (2004) Magmatic sulfide deposits. Sringer, New York, p 727
Naldrett AJ, Craig JR, Kullerud G (1967) The central portion of the Fe-Ni-S system and its bearing on pentlandite exsolution in iron-nickel sulfide ores. Econ Geol 62:826–847
Orejana D, Villaseca C (2008) Heterogeneous metasomatism in cumulate xenoliths from the Spanish Central System: implications on percolative fractional crystallization of lamprophiric melts. In: Coltorti M, Grégoire M (Eds.) Metasomatism in oceanic and continental lithospheric mantle. Geological Society of London Special Publication 293:101–120
Orejana D, Villaseca C, Paterson BA (2006) Geochemistry of pyroxenitic and hornblenditic xenoliths in alkaline lamprophyres from the Spanish Central System. Lithos 86:167–196
Orejana D, Villaseca C, Paterson BA (2007) Geochemistry of mafic phenocrysts from alkaline lamprophyres of the Spanish Central System: implications on crystal fractionation, magma mixing and xenoliths entrapment within deep magma chambers. Eur J Mineral 19:817–832
Orejana D, Villaseca C, Billström K, Paterson BA (2008) Petrogenesis of Permian alkaline lamprophyres and diabases from the Spanish Central System and their geodynamic context within western Europe. Contrib Miner Petrol 156:457–500
Orejana D, Villaseca C, Pérez-Soba C, López-García JA, Billström K (2009) The Variscan gabbros from the Spanish Central System: a case for crustal recycling in the sub-continental lithospheric mantle? Lithos 110:262–276
Orejana D, Villaseca C, Merino Martínez E (2017) Basic Ordovician magmatism of the Spanish Central System: Constraints on the source and geodynamic setting. Lithos 284–285:608–624
Orejana D, Villaseca C, Kristoffersen M (2020) Geochemistry and geochronology of mafic rocks from the Spanish Central System: Constraints on the mantle evolution beneath central Spain. Geosci Front 5:1651–1667
Piña R, Gervilla F, Barnes SJ, Ortega L, Lunar R (2013) Platinum-group elements-bearing pyrite from the Aguablanca Ni-Cu sulphide deposit (SW Spain): a LA-ICP-MS study. Eur J Mineral 25:241–252
Piña R, Romeo I, Ortega L, Lunar R, Capote R, Gervilla F, Tejero R, Quesada C (2008) Origin and emplacement of the Aguablanca magmatic Ni-Cu-(PGE) sulfi de deposit, SW Iberia: A multidisciplinary approach. GSA Bull 122:915–925
Pokrovski GS, Akinfiev NN, Borisova AY, Zotov AV, Kouzmanov K (2014) Gold speciation and transport in geological fluids: insights from experiments and physical-chemical modelling. In: Garofalo PS, Ridley JR (Eds.) Gold-transporting hydrothermal fluids in the Earth's crust. Geological Society of London Special Publication 402:9–70
Rock NMS (1991) Lamprophyres. Blackie, Glasgow, p 285
Rock NMS, Groves DI (1988) Do lamprophyres carry gold as well as diamonds? Nature 332:253–255
Romer RL, Kroner U (2018) Paleozoic gold in the Appalachians and Variscides. Ore Geol Rev 92:475–505
Sá JHS, Barnes S-J, Prichard HM, Fisher PC (2005) The distribution of base metals and platinum-group elements in magnetitite and its host rocks in the Rio Jacaré Intrusion, northeastern Brazil. Econ Geol 100:333–348
Schettino E, Marchesi C, González-Giménez JM, Saunders E, Hidas K, Gervilla F, Garrido CJ (2022) Metallogenic fingerprint of a metasomatized lithospheric mantle feeding gold endowment in the western Mediterranean basin. GSA Bull 134:1468–1484
Smith D (1995) Chlorite-rich ultramafic reaction zones in Colorado Plateau xenoliths: recorders of sub-Moho hydration. Contrib Miner Petrol 121:185–200
Tassara S, González-Jiménez J, Reich M, Schilling M, Morata D, Begg G, Saunders J, Griffin W, O'Reilly S, Grégoire M, Barra F, Corgne

A (2017) Plume-subduction interaction forms large auriferous provinces. Nat Commun 8:843

Villaseca C, Orejana D, Pin C, López-García JA, Andonaegui P (2004) Le magmatisme basique hercynien et post-hercynien du Système Central Espagnol: essai de caractérisation des sources mantelliques. Comptes Rendus Geosciences 336:877–888

Villaseca C, Orejana D, Higueras P, Pérez-Soba C, García Serrano J, Lorenzo S (2022) The evolution of the subcontinental mantle beneath the Central Iberian Zone: Geochemical tracking of its mafic magmatism from the Neoproterozoic to the Cenozoic. Earth Sci Rev 228:103997

Wang CY, Prichard HM, Zhou MF, Fisher PC (2008) Platinum-group minerals from the Jinbaoshan Pd–Pt deposit, SW China: evidence for magmatic origin and hydrothermal alteration. Miner Deposita 43:791–803

Wang Z, Cheng H, Zong K, Geng X, Liu Y, Yang J, Wu F, Becker H, Foley S, Wang CY (2020) Metasomatized lithospheric mantle for Mesozoic giant gold deposits in the North China craton. Geology 48:169–173

Wang X, Wang Z, Cheng H, Zong K, Wang CY, Ma L, Cai Y-C, Foley S, Hu Z (2022) Gold endowment of the metasomatized lithospheric mantle for giant gold deposits: Insights from lamprophyre dykes. Geochim Cosmochim Acta 316:21–40

Webber AP, Roberts S, Taylor RN, Pitcairn IK (2012) Golden plumes: substantial Au enrichment of oceanic crust during ridge-plume interaction. Geology 41:87–90

Wilson M (1989) Igneous petrogenesis: A global tectonic approach. Unwin Hyman, Boston, p 466

Zhou MF (1994) PGE distribution in 2.7 Ga layered komatiite flows from the Belingwe greenstone belt. Zimbabwe Chemical Geology 118:155–172